Electronic Supplementary Material (ESI) for RSC Advances.

Supporting Information

Photochemical Synthesis and Characterization of Novel Samarium Oxide Nanoparticles: Toward a Heterogeneous Brønsted Acid Catalyst

G. K. Hodgson, S. Impellizzeri, G. L. Hallett-Tapley and Juan C. Scaiano

Department of Chemistry and Centre for Catalysis Research and Innovation, University of Ottawa, 10 Marie Curie, Ottawa, Ontario K1N 6N5, Canada

Experimental Protocols

Photochemical synthesis of Sm_2O_3NP. Sm_2O_3NP were prepared by photochemical partial reduction of samarium nitrate hexahydrate in dry CH_3CN, *via* UVA irradiation of the benzoin Irgacure-2959™ (I-2959) photoinitiator (Scheme 1) followed by spontaneous air oxidation. Samples of I-2959 were a generous gift from Ciba Specialty Chemicals Inc. Unless otherwise noted, all other reagents and solvents were obtained from Sigma Aldrich or Fisher Scientific. Irradiation time was varied according to reaction volume, path length and reagent concentrations, with 48 h of UVA irradiation proving optimal for a 3:1 mM ratio of I-2959: $Sm(NO_3)_3 \bullet 6H_2O$ in 250 mL CH_3CN. Pertinent amounts of $Sm(NO_3)_3 \bullet 6H_2O$ and I-2959 were weighed out on an analytical balance (Sartorius model 1702) and immediately added to dry CH_3CN provided by a bench top solvent purification system (LC Technology Solutions Inc. model SPBT-1), into a freshly clean, oven-dried Pyrex test tube. A magnetic stir bar was added before the reaction vessel was fitted with a black rubber stopper and sealed with parafilm. The reaction was secured to a retort stand and purged with Argon for 1.5 h while stirring; this step was skipped for studies under air. It was then surrounded by three Luzchem exposure panels (model LZC-EXPO) powering a total of fifteen 8 W UVA bulbs (Hitachi model FL8-BL) and equipped with a Luzchem electronic timer (model LZC-TIM). The reaction proceeded at room temperature for the allotted time interval after which the cloudy but translucent dark orange solution was sonicated and separated into sterile 15 mL polypropylene centrifuge tubes (Fisherbrand model 05-539-12). Samples were then centrifuged at 10 000 rpm for 30 min (Sorvall Legend T Centrifuge, Thermo Electron Corporation). The transparent yellow supernatant was decanted and stored in the dark for observation. The remaining brown-orange solid was resuspended in a minimum of dichloromethane (DCM) via sonication and combined into four pre-weighed, clean, oven-dried glass test tubes. These four samples were centrifuged for 30 min at 3000 rpm (Drucker Co., Horizon model). The clear, colourless supernatent was discarded, the solid washed twice more with CH_3CN and the final product allowed to dry overnight in a fumehood before its mass was recorded.

Sm_2O_3NP Characterization. SEM was conducted using a JEOL JSM-7500F field emission scanning electron microscope where a drop of Sm_2O_3NP suspended in CH_3CN was placed onto a carbon film coated Cu mesh grid (Electron Microscopy Sciences model CF-400-Cu) and evaporated under ambient conditions. Sample preparation was the same for TEM imaging, which was conducted on a JEOL JEM-2100F field emission TEM operating at 200 kV. XPS was performed at the John L. Holmes Mass Spectrometry facility (University of Ottawa, Canada), using an Axis Ultra DLD X-ray photoelectron spectrometer (Kratos Analytical) with a monochromatic Al Kα X-ray source, operated at 140 W and 10^{-9} Torr. The XPS survey was obtained using a pass energy of 80 eV and an acquisition time of 342 s. High resolution Sm 3d, O 1s and C 1s XPS spectra were obtained using a pass energy of 20 eV and an acquisition time of 401 s. Analysis of XPS spectra was conducted using standard CasaXPS software (version 2.3.15). The positions of peaks were corrected using 284.5 eV as a reference value for the core level C 1s peak. XRD analysis was carried out using a Rigaku model Ultima IV X-ray diffractometer with a CuKα source, and was performed at the uOttawa X-ray core facility. Zeta potential and DLS measurements were performed on Sm_2O_3NPs dissolved in DMSO (2 mg/mL) using a Zetasizer Nano-ZS (Malvern Instruments, 633 nm laser) at 20°C. Samples were housed in a 1.0 cm path length Zetasizer Nano Series Dip Cell. FTIR Spectroscopy of Sm_2O_3NP before and after pyridine adsorption was carried out using a Nicolet 6700 FTIR spectrophotometer (Thermo Scientific) equipped with an Attenuated Total Reflectance (ATR) adapter to facilitate solid sample examination. Spectra were obtained from 500-4000 cm^{-1} at 64 scans with a resolution of 4 cm^{-1}. Samples were pre-treated at 120°C for 4 h under vacuum in a Lindeberg Blue M oven. The FTIR spectrum of pyridine was obtained using an ABB Bomem MB100 FTIR spectrophotometer at 120 scans, with a resolution of 4 cm^{-1}. Sample preparation involved suspending a mixture of liquid pyridine with Nujol mineral oil between two KBr disks. Other equipment used for the characterization of Sm_2O_3NP included: an energy-dispersive X-ray spectrometer (Oxford Instruments); a Bruker Avance 300 for ^{1}H NMR spectroscopy; a Varian Cary 50 Bio UV-visible spectrophotometer and a Photon Technology International fluorimeter. Elemental analysis was carried out using a Micro Cube Elemental Analyser (Elementar, Germany)

and was conducted by G. G. Hatch Isotope Laboratories, Earth Sciences Department, Faculty of Science, University of Ottawa, Canada.

Synthesis. Compound **1** was synthesized according to literature procedures (Ref. 19 of the main text). All reactions were monitored by thin-layer chromatography, using aluminum sheets coated with silica (60, F_{254}). NMR spectra were recorded at room temperature with a Bruker Avance 300 NMR spectrometer. Mass spectral analysis was performed with a 6890N Network GC System equipped with a 5973 Mass Selective Detector from Agilent Technologies. ESI mass spectra in positive mode were acquired with a Micromass Q-TOF I. High-resolution EI mass spectra were acquired with a HRes, Concept S1, Magnetic Sector mass spectrometer and were conducted in the John L. Holmes Mass Spectrometry Facility at the Department of Chemistry, University of Ottawa, Canada.

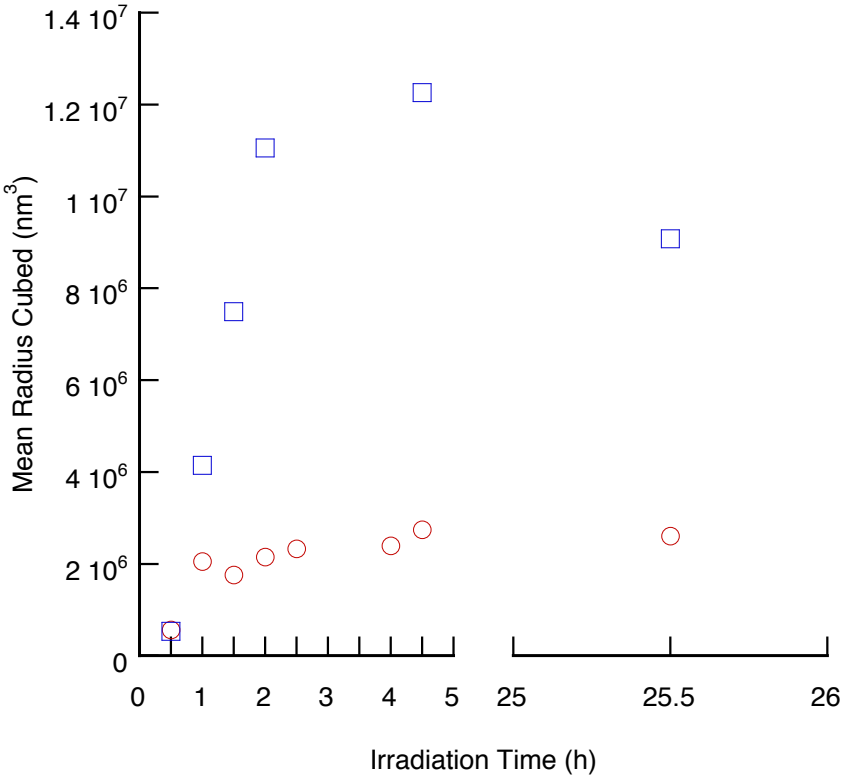

Figure S1 DLS performed at regular intervals during the photochemical synthesis of Sm_2O_3NP. Irradiation was consistently interrupted in order to obtain each measurement. Red circles represent the formation of Sm_2O_3NP in CH_3CN under Ar (g) and blue squares represent the data obtained when the synthesis was performed under air.

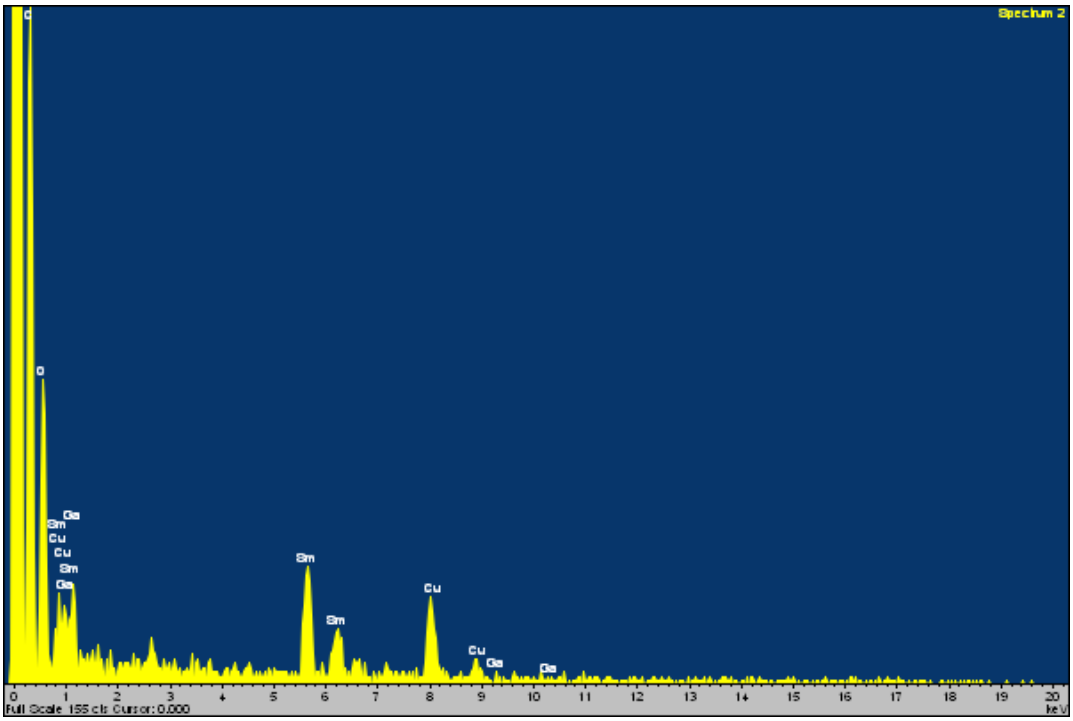

Figure S2 EDS spectrum of Sm_2O_3NP.

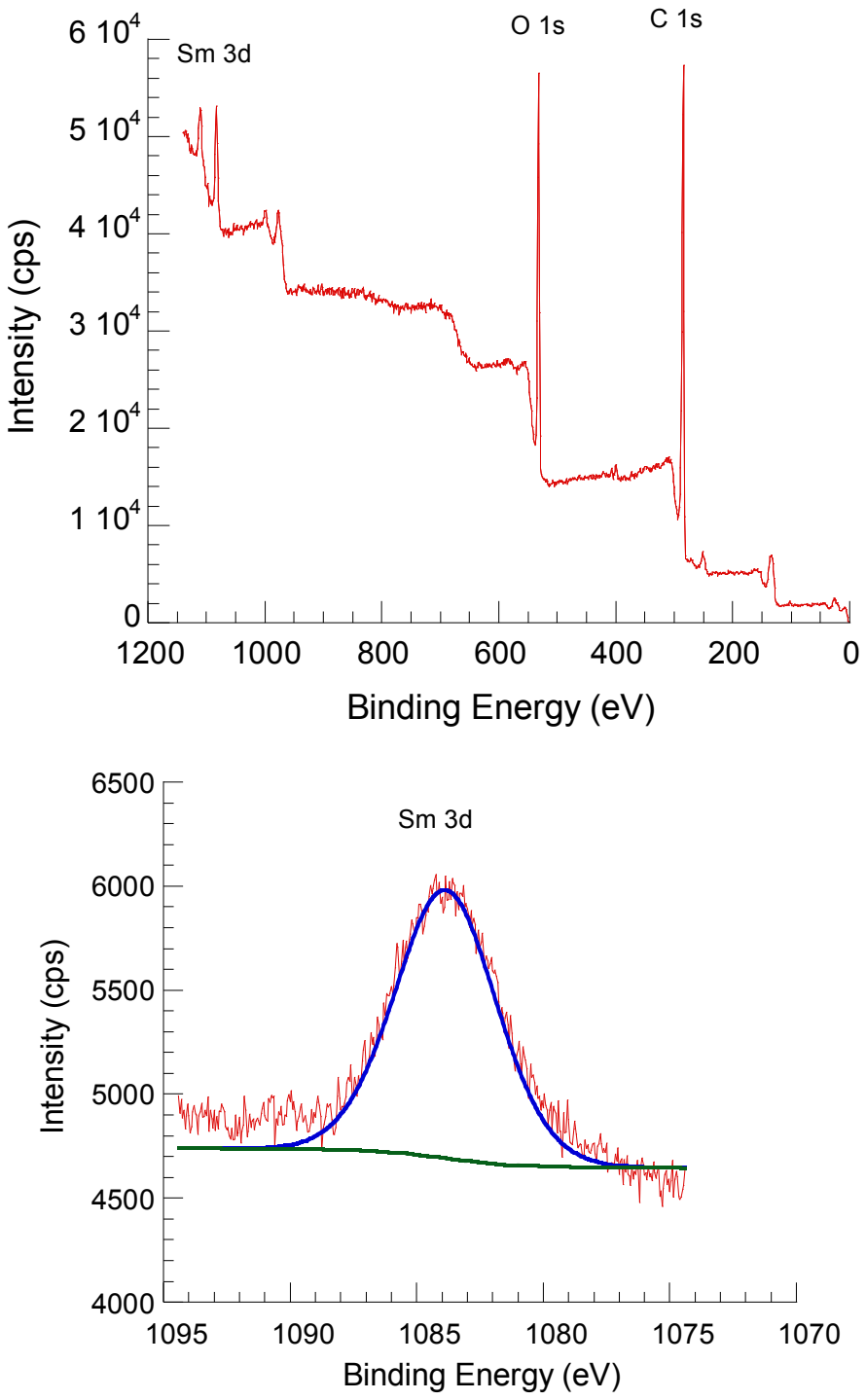

Figure S3 *Upper panel*: XPS spectrum over a broad range of binding energies. *Lower panel*: core level Sm 3d XPS spectrum of Sm_2O_3NP showing one of the characteristic Sm^{3+} peaks centred at 1084.0 eV.

Details of XPS Interpretation. Hyperfine splitting of each Sm_2O_3 peak or the presence of shoulders can sometimes be observed and is often attributed to the presence of ionic Sm^{2+} (*i.e.* SmO) or metallic samarium.[1,2] The relative proportions of Sm^0, SmO and Sm_2O_3, which can change as samarium undergoes oxidation, are then discussed according to the relative intensity of their apparent peaks. However, this form of interpretation can be misleading as it often requires extensive peak deconvolution incorporating arbitrary constraints on fitting parameters. Thus, beyond assuming a Gaussian shape, the XPS spectrum of bulk samarium metal will invariably display similar peak splitting and shoulder components.[3-5] Although the Binding Energy (BE) of the Sm^{2+} signal is generally considered to fall between those of Sm^{3+} and Sm^0, conflicting reports concerning whether the peaks ascribed to SmO appear at higher or lower BE relative to the Sm_2O_3 doublet depending upon the attributes of the material (*e.g.* support, dopant, preparation method) further draw the reliability of such analyses into question. Even if fitting methods did not suffer from these drawbacks, samarium is redox-active and the surfaces of samarium oxide materials have been reported to rapidly change oxidation states (a potential asset in catalysis) while the interior remains as Sm_2O_3.[4,7] Further, surface SmO could easily be generated in situ *via* reduction of Sm^{3+} initiated by bombardment with high-energy X-rays during XPS spectral acquisition. Unfortunately in this case the core level O 1s XPS spectrum could not provide any additional insight regarding the presence or absence of Sm^{2+}. Although spin-orbit splitting observed in this region can, in principle, be related to the ratio of O–Sm^{2+}/O–Sm^{3+}/surface OH groups,[1,2,6] the degree of splitting was insufficient for a reliable deconvolution procedure to be attempted. It is important to note that interpretation of the O 1s and C 1s peaks should be made with caution, as sample contamination from adsorbed atmospheric oxygen and carbon can enhance measured intensity. Suffice to say that the lack of an excess of samarium with respect to oxygen qualitatively corroborates the identification of the material as Sm_2O_3.

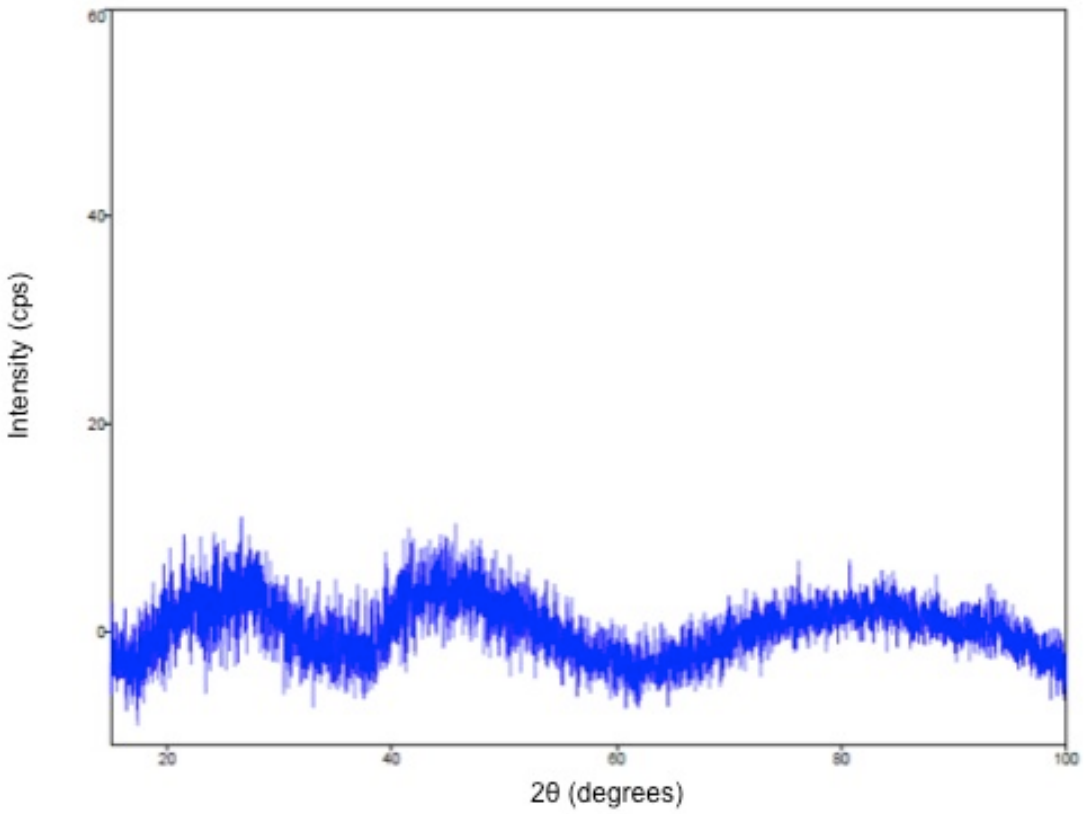

Figure S4 XRD spectrum of Sm_2O_3NP showing typical peak broadening associated with amorphous solid nanostructures.

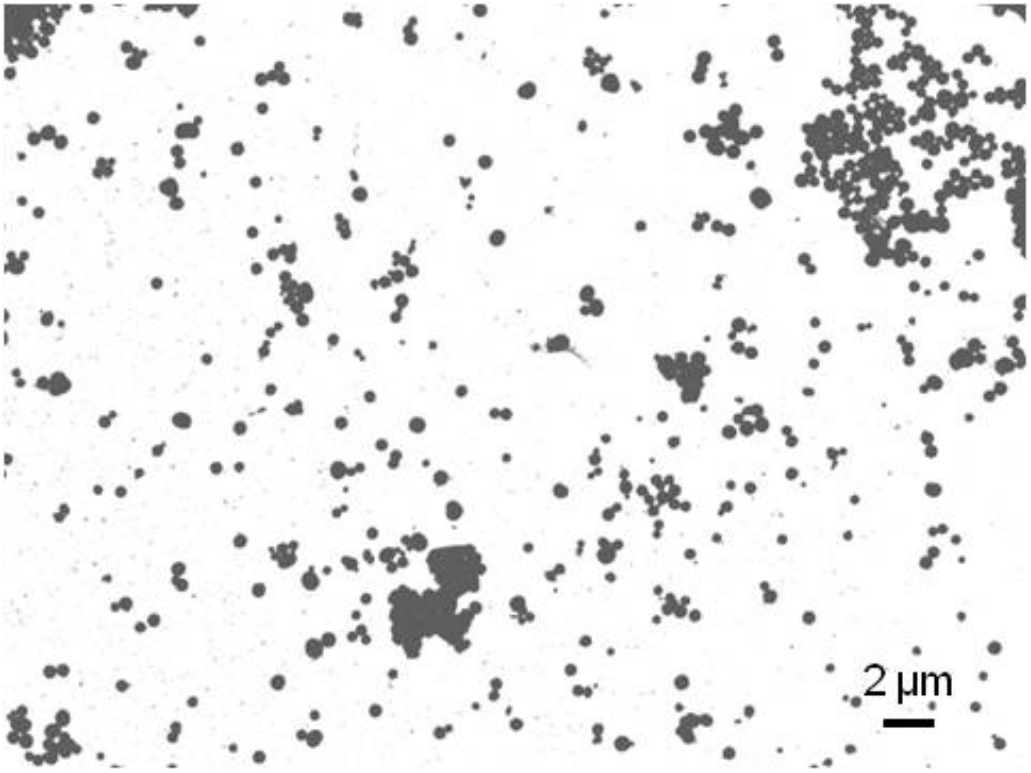

Figure S5 SEM image of Sm_2O_3NP used for particle sizing represented in Figure 1.

Table S1 Raw DLS data pertaining to three samples of 2 mg/mL Sm_2O_3NP dissolved in DMSO (absorbance = 0.085 at 650 nm).

Sample	Run	Hydrodynamic Diameter (nm)
1	1	734.0
1	2	466.4
1	3	605.1
2	1	385.2
2	2	571.3
2	3	374.2
3	1	498.6
3	2	574.5
3	3	381.9
Mean (nm)	510.1	
Standard Devation	122.3	

Table S2 Elemental analysis of Sm_2O_3NP performed in duplicate.

Mass (mg)	Carbon	Hydrogen	Nitrogen	Sulfur
4.391	37.80	4.05	2.62	0.32
4.823	37.74	4.75	2.65	0.32

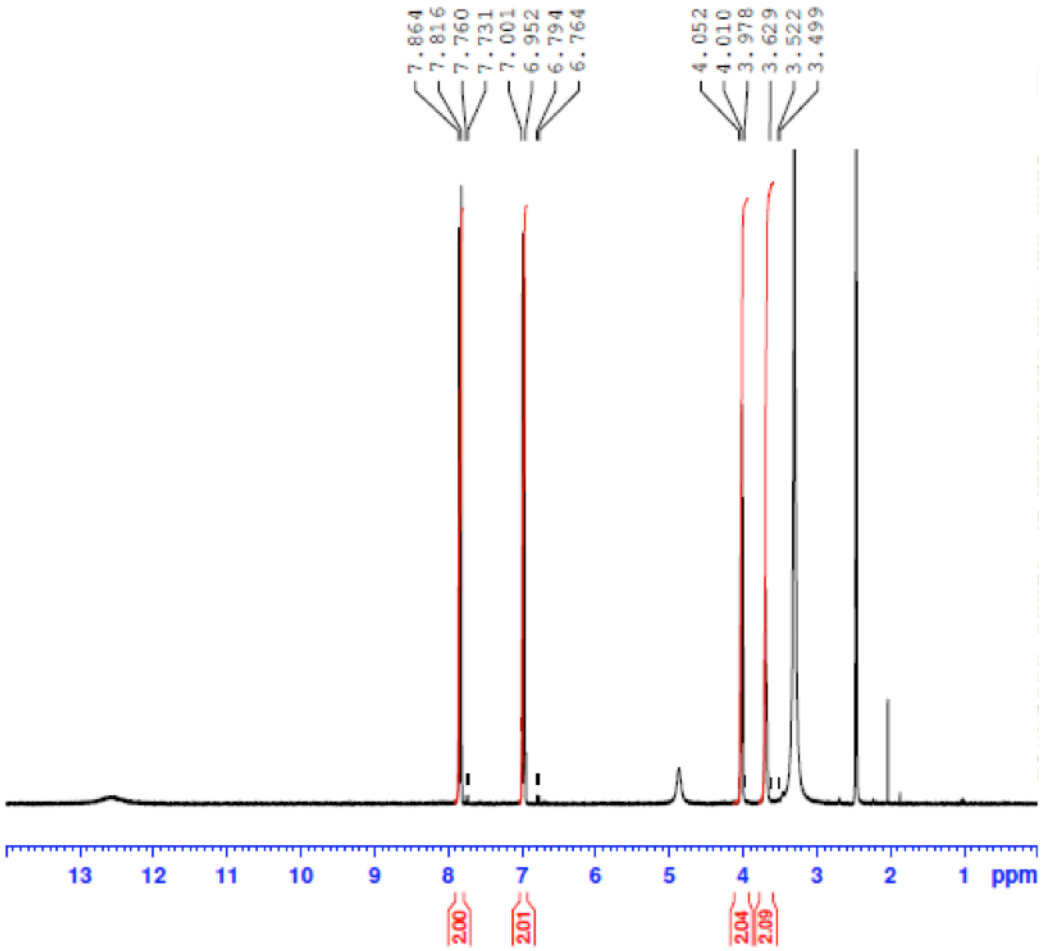

Figure S6 ^{1}H NMR spectrum of 4-HEBA in DMSO-d_6.

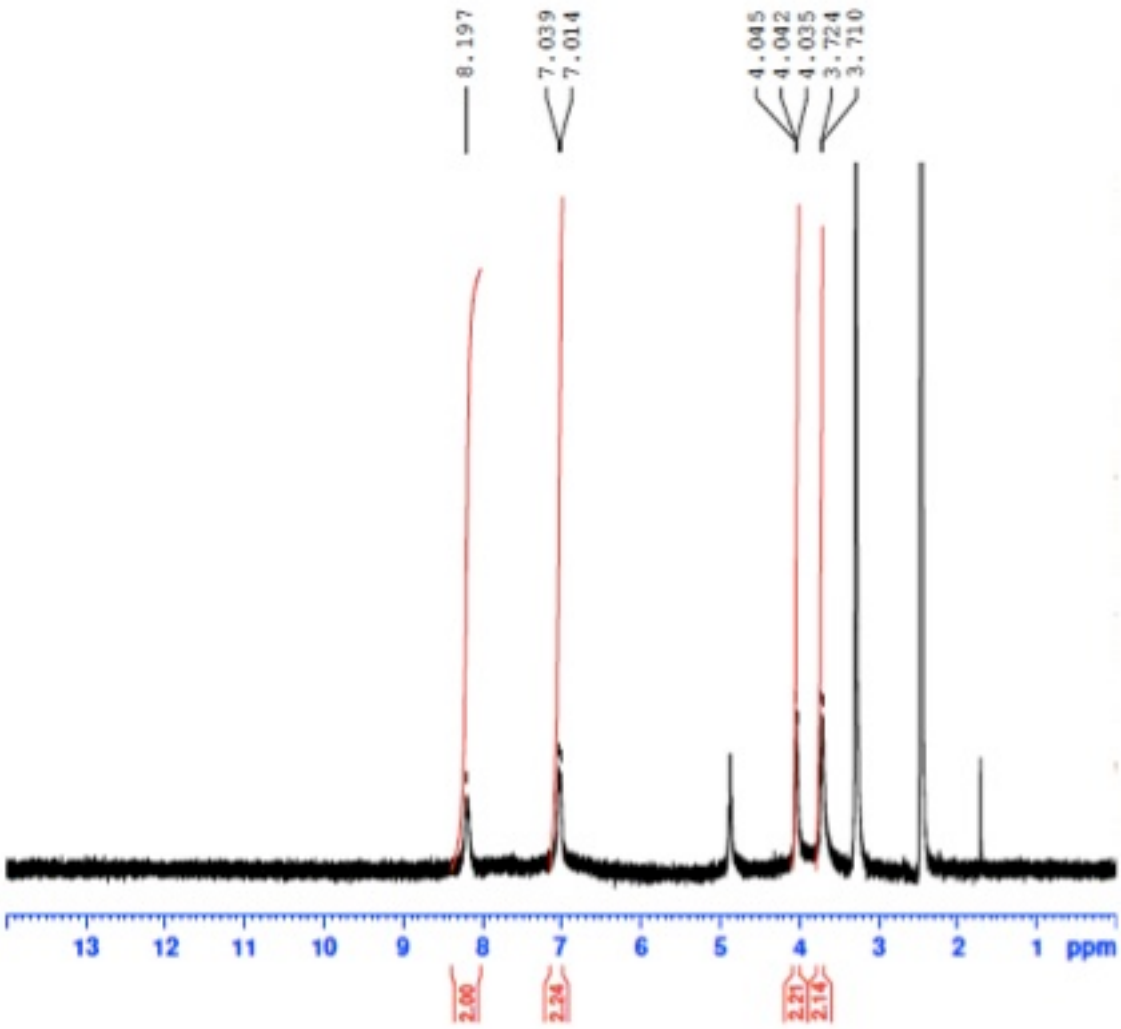

Figure S7 ^{1}H NMR spectrum of Sm_2O_3NP in DMSO-d_6.

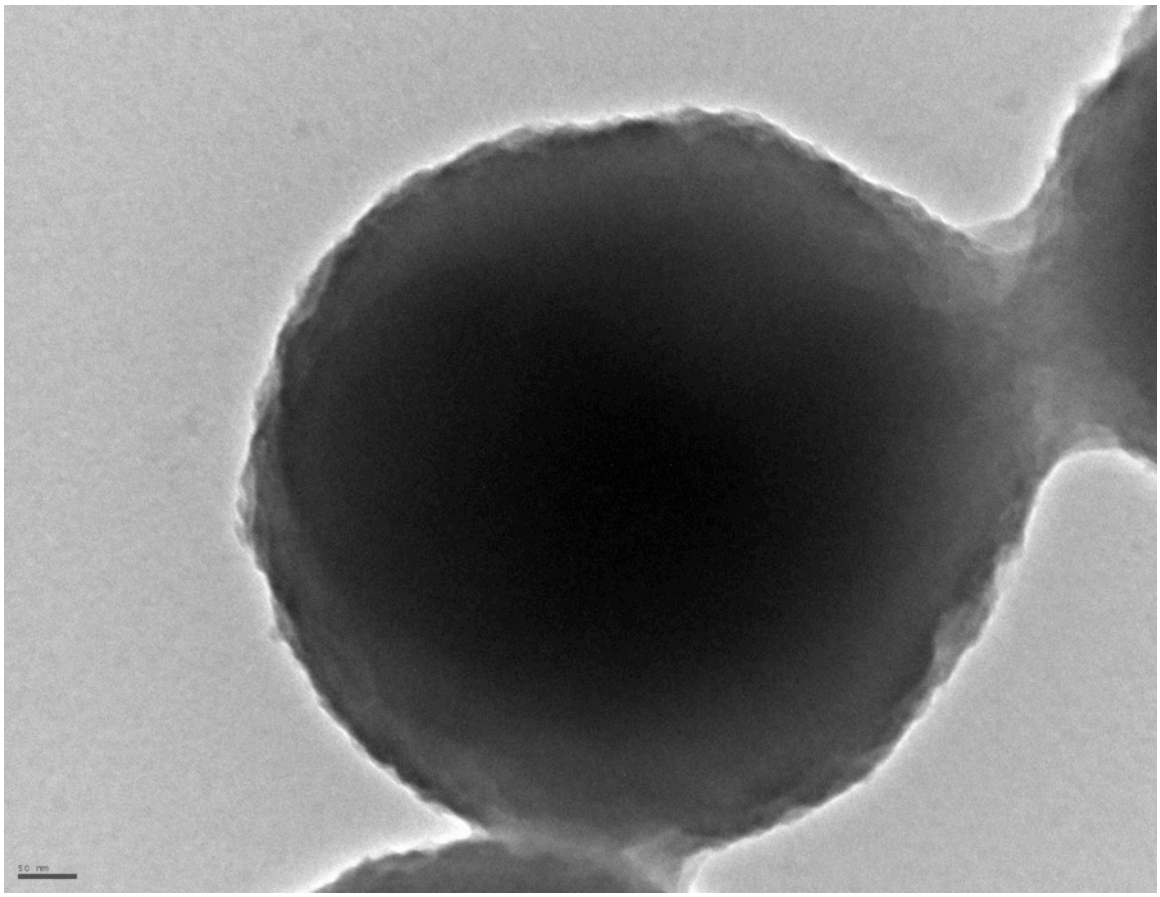

Figure S8 TEM image of Sm_2O_3NP, showing that each particle is not made up of smaller NP but exists as an individual spherical unit. Scale bar = 50 nm. Image obtained on a JEOL JEM-2100F Field Emission TEM operating at 200 kV.

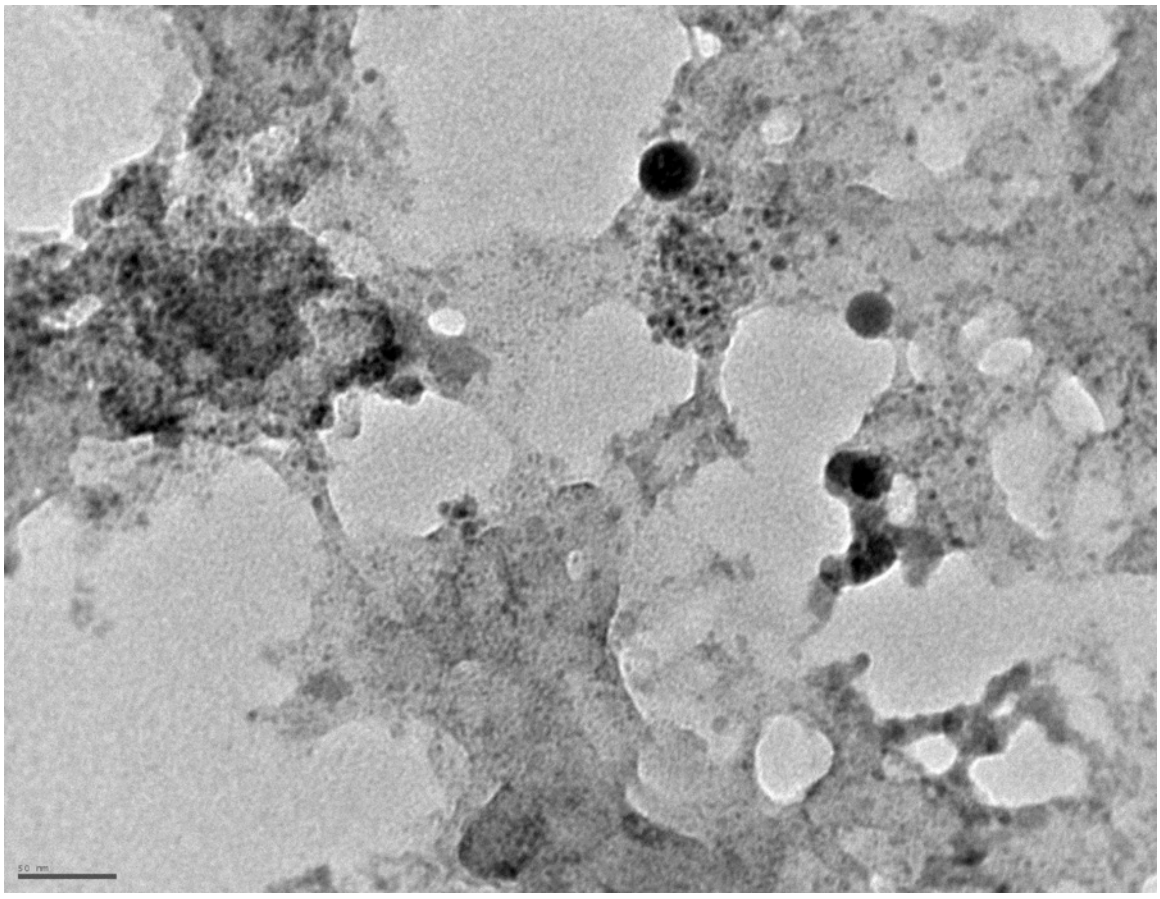

Figure S9 TEM image showing the raw results of laser drop ablation performed on a 0.88 mg/mL suspension of Sm_2O_3NP in MilliQ H_2O prior to purification.[8] Laser drop ablation conditions: 355 nm, 5 Hz, 5 pulses/drop. Image obtained on a JEOL JEM-2100F Field Emission TEM operating at 200 kV. Scale bar = 50 nm.

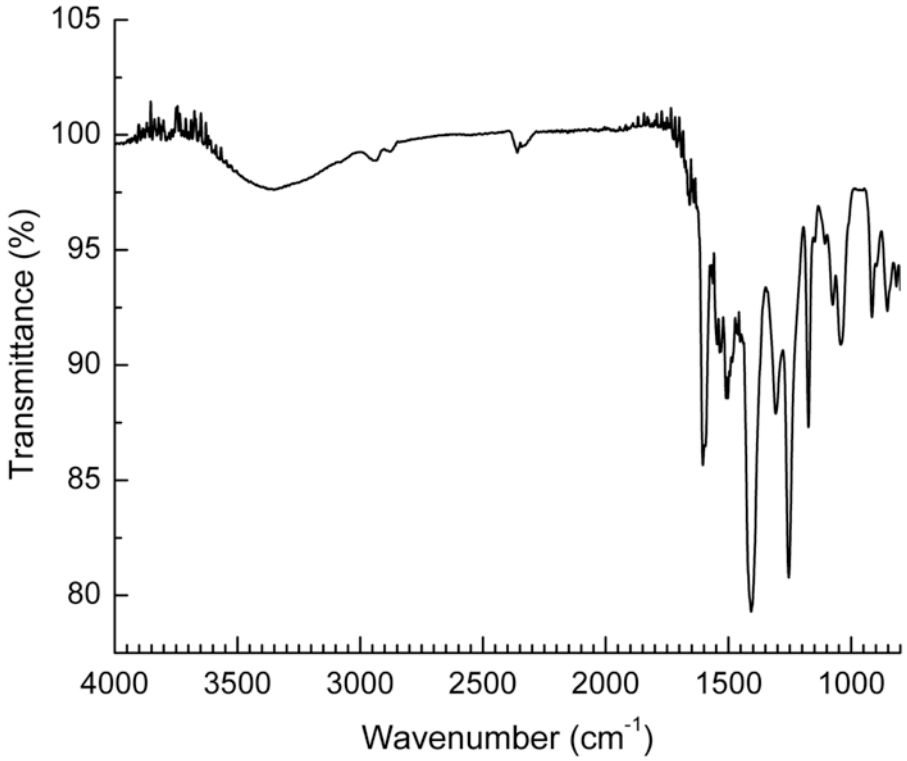

Figure S10 Full-scale FTIR spectrum of solid Sm_2O_3NP before exposure to pyridine vapour.

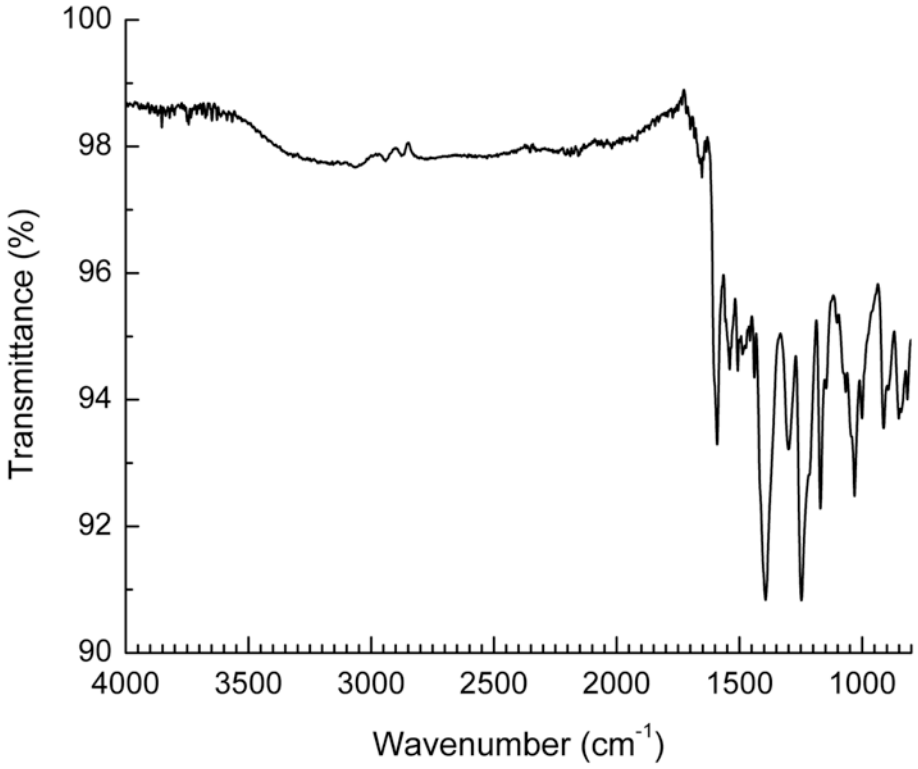

Figure S11 Full-scale FTIR spectrum of solid Sm_2O_3NP saturated with adsorbed pyridine vapour.

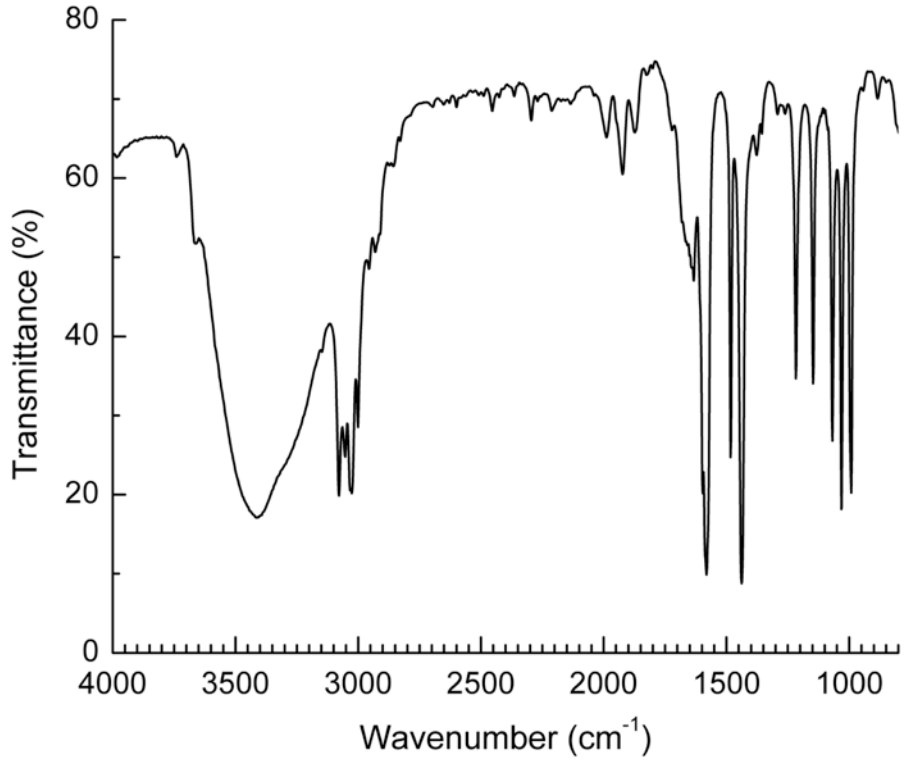

Figure S12 Full-scale FTIR spectrum of pyridine. A liquid sample was prepared in Nujol mineral oil and the spectrum obtained from 500-4000 cm^{-1} at 120 scans, with a resolution of 4 cm^{-1}.

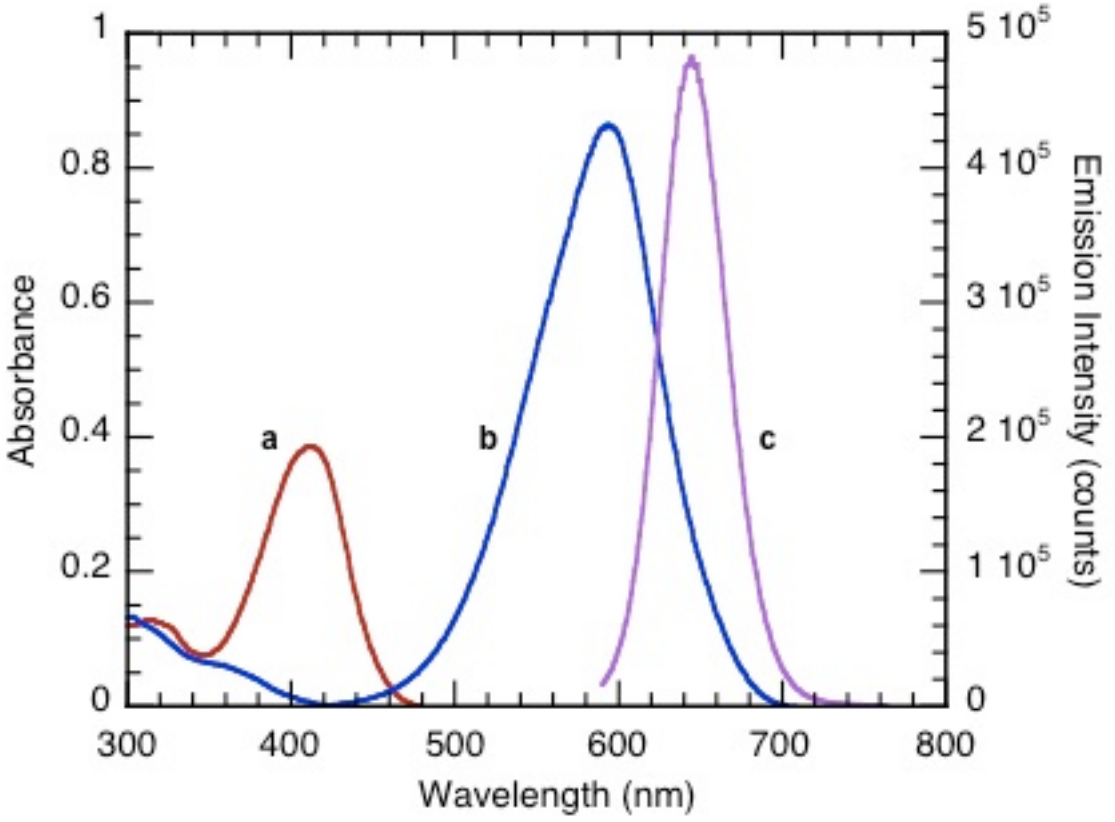

Figure S13 Absorption spectra of **1** (10 μM, CH_3CN, 25 °C) before (**a**) and after (**b**) the addition of 10 equivalents of TFA. Emission spectrum (**c**, λ_{Ex} = 570 nm, CH_3CN, 25 °C) of **1** after the addition of 10 equivalents of TFA.

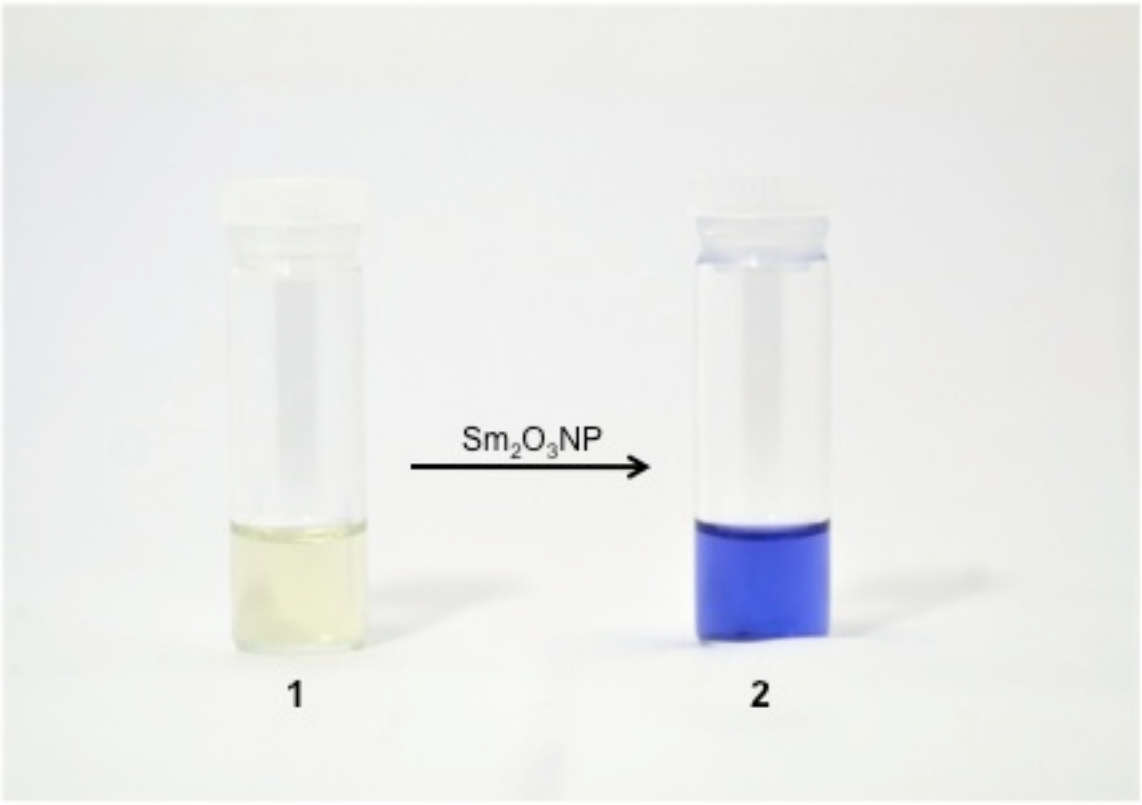

Figure S14 Image showing the conversion from **1** (left) to **2** (right) caused by acid-induced ring opening owing to the Brønsted acidity of Sm_2O_3NP.

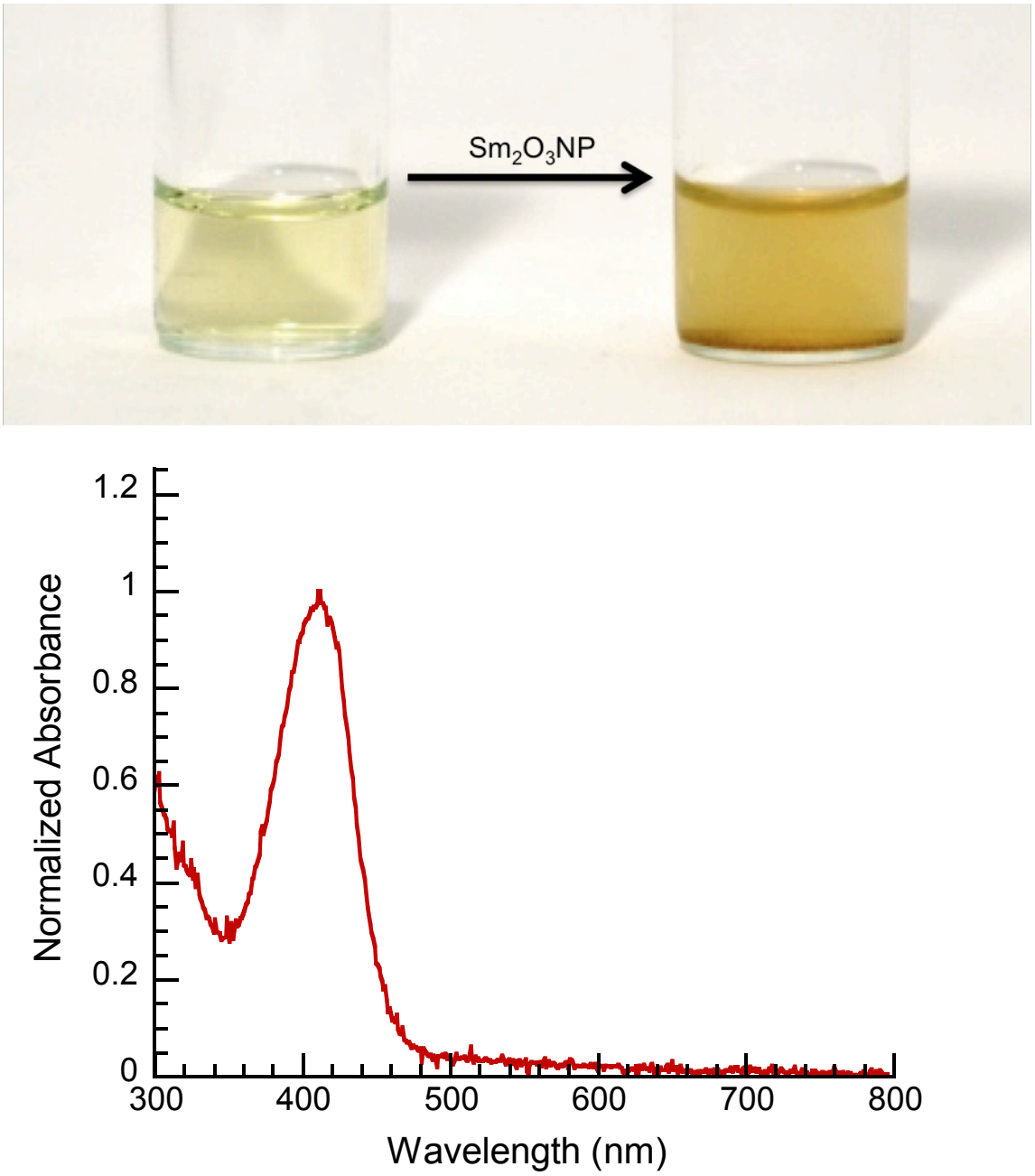

Figure S15 *Upper panel*: image of a 10 µM solution of **1** before (left) and 24 h after (right) addition of base treated Sm_2O_3NP. *Lower Panel:* normalized absorbance of a 10 µM solution of **1** after 24 h exposure to base treated Sm_2O_3NP and subsequent centrifugation. Note the lack of absorbance at 590 nm that would be indicative of the presence of **2**.

References:

1. T.-D. Nguyen, D. Mrabet and T.-O. Do, *J. Phys. Chem. C*, 2008, 112, 15226-15235.
2. T.-D. Nguyen, C.-T. Dinh and T.-O. Do, *Langmuir*, 2009, 25, 11142-11148.
3. M. G. Mason, S. T. Lee, G. Apai, R. F. Davis, D. A. Shirley, A. Franciosi and J. H. Weaver, *Phys. Rev. Lett.*, 1981, 47, 730-733.
4. Q. Xu, S. Hu, D. Cheng, X. Feng, Y. Han and J. Zhu, *J. Chem. Phys.*, 136, -.
5. D. D. Sarma, M. S. Hegde and C. N. R. Rao, *J. Chem. Soc., Faraday Trans. 2*, 1981, 77, 1509-1520.
6. F. Zhang, P. Wang, J. Koberstein, S. Khalid and S.-W. Chan, *Surf. Sci.*, 2004, 563, 74-82; T. He, D. Chen, X. Jiao, Y. Wang and Y. Duan, *Chem. Mat.*, 2005, 17, 4023-4030.
7. D. Cheng, Q. Xu, Y. Han, Y. Ye, H. Pan and J. Zhu, *J. Chem. Phys.*, 140, -.
8. C. J. Bueno-Alejo, C. D'Alfonso, N. L. Pacioni, M. Gonzalez-Bejar, M. Grenier, O. Lanzalunga, E. I. Alarcon and J. C. Scaiano, *Langmuir*, 2012, *28*, 8183-8189.